Stimuli-responsive polyaniline coated silica microspheres and their electrorheology

2016 Smart Mater. Struct. 25 055020

(http://iopscience.iop.org/0964-1726/25/5/055020)

IOP Publishing Smart Materials and Structures
Smart Mater. Struct. 25 (2016) 055020 (11pp) doi:10.1088/0964-1726/25/5/055020

Stimuli-responsive polyaniline coated silica microspheres and their electrorheology

Dae Eun Park[1], Hyoung Jin Choi[1] and Cuong Manh Vu[2]

[1] Department of Polymer Science and Engineering, Inha University, Incheon, 402-751, Korea
[2] Chemical Department, Le Qui Don Technical University, No.236 Hoang Quoc Viet, Ha Noi, Vietnam

E-mail: hjchoi@inha.ac.kr

Received 20 December 2015, revised 26 February 2016
Accepted for publication 3 March 2016
Published 7 April 2016

Abstract

Silica/polyaniline (PANI) core–shell structured microspheres were synthesized by coating the surface of silica micro-beads with PANI and applied as a candidate inorganic/polymer composite electrorheological (ER) material. The silica micro-beads were initially modified using N-[(3-trimethoxysilyl)-propyl] aniline to activate an aniline functional group on the silica surface for a better PANI coating. The morphology of the PANI coating on the silica surface was examined by scanning electron microscopy and the silica/PANI core–shell structure was confirmed by transmission electron microscopy. The chemical structure of the particles was confirmed by Fourier transform infrared spectroscopy. Rotational rheometry was performed to confirm the difference in the ER properties between pure silica and silica/PANI microsphere-based ER fluids when dispersed in silicone oil.

Keywords: electrorheological, core–shell, polyaniline, microsphere

(Some figures may appear in colour only in the online journal)

1. Introduction

A range of synthesis methods and applications of inorganic/polymer composite materials, such as hollow or core–shell structural particles, nanotubes, nanofibers, nanoparticles, and ultrathin films, have been introduced [1–3], due to the synergic effects from the advantages of both polymers and inorganic materials. Some examples include inorganics, such as SiO_2, Fe_3O_4, TiO_2, and clay and conducting polymer composites [4–6], from different fabrication methods [7–10] of solvent casting, blending, *in situ* polymerization, pickering free emulsifier emulsion polymerization.

Concurrently, electric-stimuli responsive electrorheological (ER) fluids have attracted increasing attention as smart suspensions, which are composed of electric-stimuli semi-conducting and/or dielectric particles dispersed in non-conducting liquids. They can be altered from a liquid-like to a solid-like state [7] after the application of an electric field strength. When the electric field strength is applied, the randomly dispersed particles are polarized due to dielectric constant mismatch between the particles and medium [9]. The dipole–dipole interaction among polarized particles aligns themselves to arrange in the form of a chain, which alters their rheological properties dramatically [11, 12]. Owing to the rapid reversible and tunable response under an electric field, ER fluids are used in a range of engineering applications, such as ER valve, clutches, engine mounts, shock absorbers, and ER tactile displays [13–16].

Many electro-responsive materials have been examined because of their smart and intelligent characteristics with industrial potential. In particular, inorganic/polymer hybrids for ER fluids have attracted more attention than either pure inorganic or polymers, such as polymer/mesoporous materials, clay/polymer nanocomposites and core–shell structured materials [3, 17–20]. In addition, the particle size and shape have important effects on the ER properties [21]. Therefore, the core–shell structure has gained special attention because of their advantages on the ER performance regarding the particle shape, size control, density control, and electrical conductivity control.

One of the most attractive conducting polymers is polyaniline (PANI) because of its environmental stability, low cost, controllable conductivity, and relatively lower density. On the other hand, PANI still requires improvement before it can be used as an ER fluid in commercial products due to several intrinsic problems, such as high current density and

colloidal instability. Therefore, many experiments on PANI/inorganic materials, such as PANI/carbon nanotube [22], PANI/clay [19, 23] and PANI/TiO_2 [24], have been carried out. Studies of PANI/silica have been also carried out using a range of methods [25–29]. Recently, Dai *et al* [30] fabricated PANI hollow microspheres with tunable nanoshell thickness using spherical silica particle as a core. Despite these studies, it is difficult to coat a silica particle surface uniformly with PANI.

In this work, a facile method was used to produce a uniform PANI coating on the silica microspheres of the core–shell structure. The silica core was introduced to provide not only spherical structural shape of the final products but also their good mechanical strength compared to pure PANI particles. For a PANI coating on the silica surface, the surface of silica particles was modified to an aniline group for π–π^* stacking interactions with aniline monomer. Furthermore, the ER properties of pure silica were compared with those of silica/PANI core–shell microspheres at the same volume fraction (20 vol%).

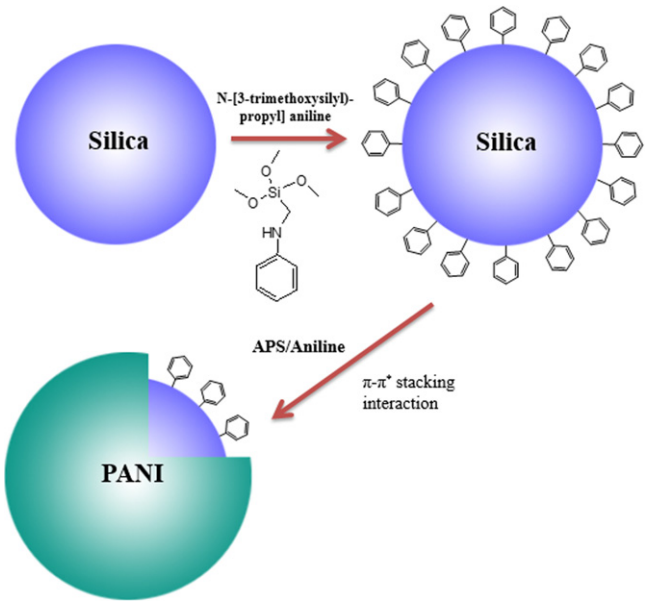

Scheme 1. Schematic diagram of the polyaniline coating on the silica surface.

2. Experimental

2.1. Materials

Silicon dioxide (SiO_2) (1 μm, 99.9%, Alfa Aesar), N-[3-trimethoxysilyl)-propyl] aniline (PAPTMS) (Aldrich), ammonium persulfate (APS) (98%, Daejung, Korea), and aniline (99%, DC Chemical, Korea) were used as received. Hydrochloric acid (HCl) (35%, Junsei Chemical, Japan) was mixed with distilled (DI)-water to make a 1 M HCl solution.

2.2. Preparation of aniline functionalized silica spheres

Silica particles (10 g) were immersed in HCl (1 M, 150 ml) and stirred for 24 h, followed by washing with DI-water and drying under vacuum at 60 °C. The particles were dispersed in toluene (150 ml), and PAPTMS (10 ml) was then added with stirring for 48 h. The surface-modified silica particles were washed with a mixture of toluene and ethanol (1:1 v/v) and dried under vacuum at 60 °C.

2.3. Preparation of SiO_2/PANI core–shell microspheres

The modified silica particles (5 g) were dispersed in DI-water (280 ml) and HCl (1 M, 120 ml) was then added by stirring with a magnetic bar. The aniline monomer (1.25 g) and APS (3.75 g) were added to the solution and stirred for 24 h. The resulting particles were washed with ethanol and DI-water, and finally dried in a vacuum at 60 °C. For the proper ER material, the electrical conductivity of silica/PANI microspheres was controlled by a dedoping process [31–33] and the pH was maintained at 10 by adding either a 1 M NaOH or 1 M HCl solutions and monitored using a pH meter (Multi 9310, WTW, Germany).

2.4. Preparation of ER fluid

To prepare an ER fluid with a 20 vol% particle concentration, the fabricated SiO_2/PANI microspheres were dispersed uniformly in silicone oil (KF-96, Shin-Etsu, kinematic viscosity: 100 cS, density: 0.975 g cm^{-3}) using a sonifier.

2.5. Characterization

The surface morphologies of both the pristine SiO_2 and SiO_2/PANI microspheres were observed by both scanning electron microscopy (SEM, S-4300, Hitachi, Japan) and transmission electron microscopy (TEM, CM 200, Philips, Netherland). The densities of both pure the silica and silica/PANI microspheres were measured using a gas pycnometer (AccuPyc 1340, Micromeritics, USA). X-ray energy dispersive spectroscopy was performed for elemental analysis using an attached EDAX spectrometer. The chemical structure was analyzed by Fourier transform infrared (FT-IR) spectroscopy (Perkin-Elmer system 2000) over the frequency range, 400–4000 cm^{-1}. The thermal properties were examined by thermal gravimetric analysis (TGA, Q50, TA Instruments, USA), in which the samples were heated from room temperature to 800 °C in air. The fibrillation phenomenon of the SiO_2/PANI microsphere-based ER fluid was tested by an optical microscopy (OM, BX51, Olympus, USA). The dielectric spectra of the silica/PANI-based ER fluid were measured using an impedance analyzer (HP4284A) with a liquid test fixture (HP16452) over the frequency range, 20 Hz–10^6 Hz. The electrical conductivity of the particles was then measured using a resistivity meter (MCP-T610, Mitsubishi, Japan), in which its conductivity of the pristine particles before the dedoping process with 1.8×10^{-2} S cm^{-1} was decreased to be 5.8×10^{-12} S cm^{-1}. The rheological properties of the ER fluid were investigated using a rotational rheometer (MCR 300, Physica, Stuttgart, Germany), which

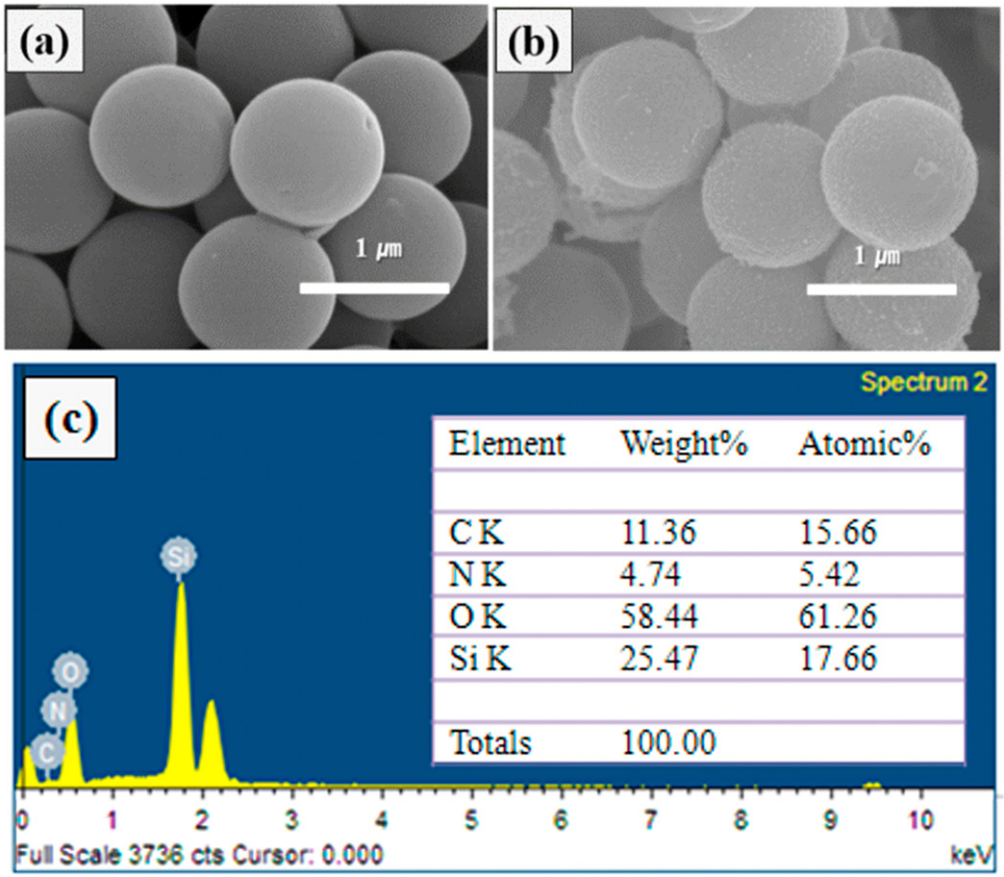

Figure 1. SEM images of pure silica (a), silica/PANI core–shell microspheres (b), and EDX spectra of the PAPTMS coated silica (c).

was equipped with a high voltage supply (Fug, HCN 7E-12 500, Germany). The cell geometry for the ER measurement was a concentric cylinder (CC17/E, Anton Paar, Germany)

3. Results and discussion

The silica/PANI core–shell structure particles were synthesized by a chemical oxidative polymerization method using the surface modified silica particles.

Scheme 1 shows the process for fabricating the PANI coating on the surface of the spherical silica beads. With the surface of silica possessing hydroxyl groups called silanol [34], the silica surface became more activated by the HCl solution. The activated silica was then dispersed in toluene and stirred with PAPTMS. As a result, the aniline functional groups were formed on the silica surface. When the modified silica was mixed with a mixture of aniline monomer and APS in DI water, PANI coated the silica surface due to π–π^* stacking interactions between the aniline functional group and aniline monomer [35]. APS was then added as an initiator and HCl was also added as aniline converted to phenyl ammonium ions. The phenyl ammonium ions were polymerized into PANI by an oxidation reaction of APS [36].

The surface morphologies of silica and silica/PANI core–shell microsphere were observed by SEM to confirm the PANI coating on the silica surface. Figure 1 shows SEM images of the pure silica (a) and silica/PANI core–shell microspheres (b). PANI coating made the silica surface rough compared to the smooth pristine silica surface. Both of pure silica and silica/PANI core–shell microsphere diameters were approximately 1 μm. This shows that the PANI coating on the silica surface was quite thin. Figure 1(c) shows the EDX spectra of PAPTMS coated silica, which confirmed the presence of the elements of PAPTMS, such as silicon, oxygen, carbon, and nitrogen. Carbon and nitrogen do not exist in the pure silica, confirming that the PAPTMS coating on silica was successful based on the EDX spectra.

The particle size distributions of the silica and silica/PANI core–shell microspheres were examined by dynamic light scattering. Figure 2 shows the light scattering intensity distribution at various particle diameters. The mean diameter of silica and silica/PANI were 988.1 nm and 1085.4 nm, respectively, indicating that the thickness of the PANI shell was approximately 50 nm. The polydispersity index (PI) was also calculated using the following equation:

$$\mathrm{PI} = \frac{\overline{d_s}}{\overline{d_n}} = \frac{(\overline{d}^2)^{\frac{1}{2}}}{\overline{d}} = \frac{(\overline{d}^2 + \sigma^2)^{\frac{1}{2}}}{\overline{d}} = \left\{1 + \left(\frac{\sigma}{\overline{d}}\right)^2\right\}^{\frac{1}{2}}. \quad (1)$$

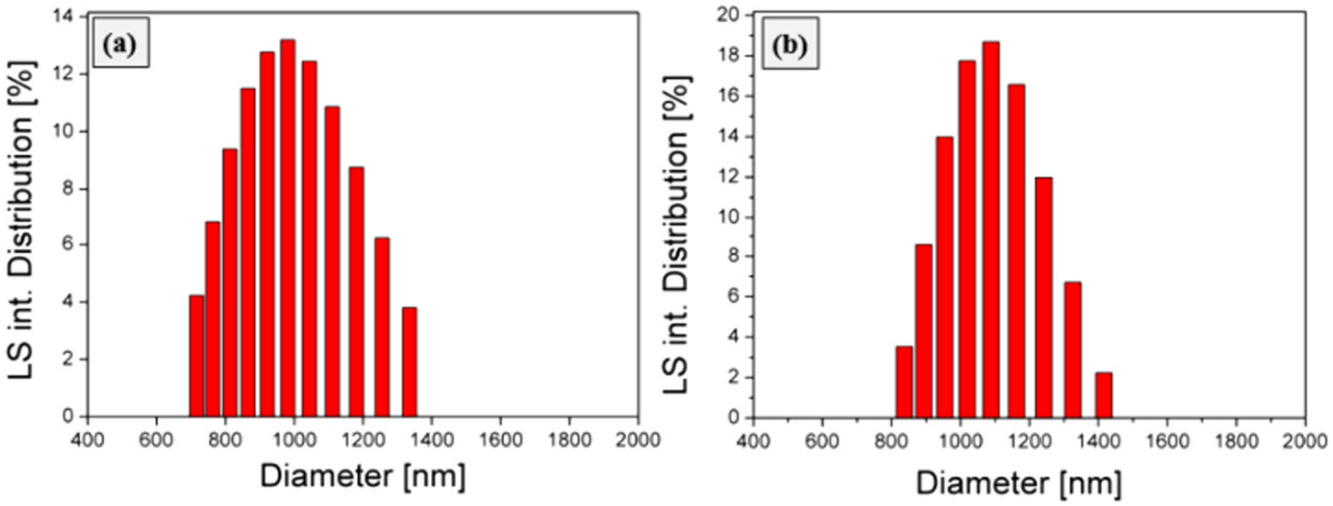

Figure 2. Light scattering intensity distribution of (a) silica and (b) silica/PANI core–shell microspheres.

$\overline{d_s}$ is an area average, $\overline{d_n}(=\bar{d})$ is a number average and σ is the standard deviation. The PI of silica and silica/PANI were 1.013 and 1.008, respectively.

The compositions of silica/PANI core–shell microspheres were confirmed by FT-IR. Figure 3 presents the FT-IR spectra of (a) PANI, (b) silica/PANI and (c) pure silica. The spectrum of PANI in figure 3(a) showed absorption bands at 1565 cm^{-1} and 1475 cm^{-1}, which were assigned to the C=N and C=C stretching, respectively. The C–N stretching band also appeared at 1292 cm^{-1} and 1245 cm^{-1}. In figure 3(c), the characteristic bands at 807 cm^{-1} and 468 cm^{-1} were assigned to the major peaks of the silica Si–O–Si stretching vibrations. Si–O–Si anti-symmetric stretching and Si–OH bending appeared at 1108 cm^{-1} and 957 cm^{-1}, respectively. Figure 3(b) clearly shows that silica/PANI core–shell microspheres have characteristic peaks for both pure silica and PANI, as shown in figures 3(a) and (c), respectively.

Figure 4 shows the core–shell structure of the silica/PANI microspheres. The thin external gray shell covered the internal black core surface. The black part is silica and the covered part is PANI. The thickness of the shell was approximately 50 nm and it did not significantly affect the size of the silica particle. The density of silica decreased after the PANI coating to 1.87 g cm^{-3} from 2.02 g cm^{-3} and the density of PANI was 1.36 g cm^{-3}. The weight ratio of the PANI shell could be calculated based on the shell thickness using equations (2.1)–(2.3) as follows [37]:

$$\frac{V_2\rho_2}{V_1\rho_1 + V_2\rho_2} \times 100\% = m, \tag{2.1}$$

$$V_1 = \frac{4}{3}\pi R^3, \tag{2.2}$$

$$V_2 = \frac{4}{3}\pi[(R+h)^3 - R^3], \tag{2.3}$$

where V_1, V_2 and ρ_1, ρ_2 are the volume and density of the silica core and PANI shell, respectively; m is the weight ratio of the PANI shell; R is the diameter of the silica; and h is the thickness of the coated PANI shell. The calculated m value was 10 wt%.

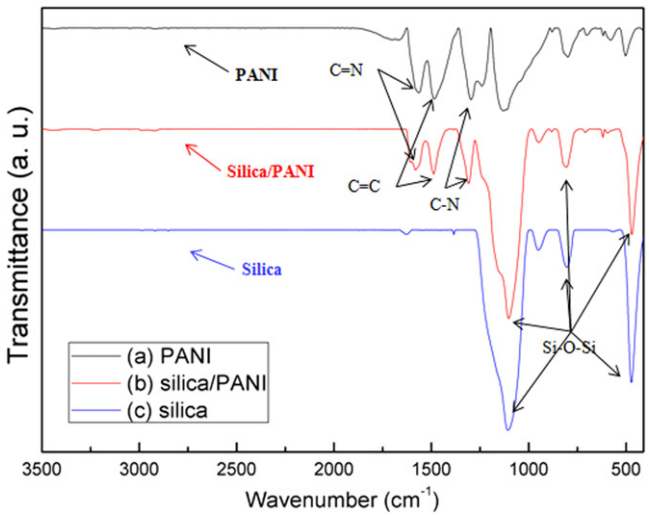

Figure 3. FT-IR spectra of PANI (a), silica/PANI core–shell microspheres (b) and pure silica (c).

The weight ratio of the PANI shell is also confirmed by TGA. Figure 5 shows the TGA results of pure silica (a), silica/PANI core–shell microspheres (b) and PANI (c). The slight weight loss before 100 °C was assigned to the adsorbed moisture in the particles. In figure 5(a), the first weight loss due to the removal of water molecules was observed until 150 °C. From 400 °C, the second weight loss was assigned to the decomposition of oxygen functional groups on the silica surface [34]. In figure 5(c), a sharp decrease in mass was observed at 300 °C due to thermal degradation of the PANI chains. In the case of silica/PANI microspheres in figure 5(b), the weight loss was attributed to both thermal degradation of the PANI chains and the decomposition of oxygen functional groups on the silica surface. Based on the data, the mass ratio of the PANI shell was estimated to be approximately 10 wt%. This value is the same as that calculated from equation (2.1).

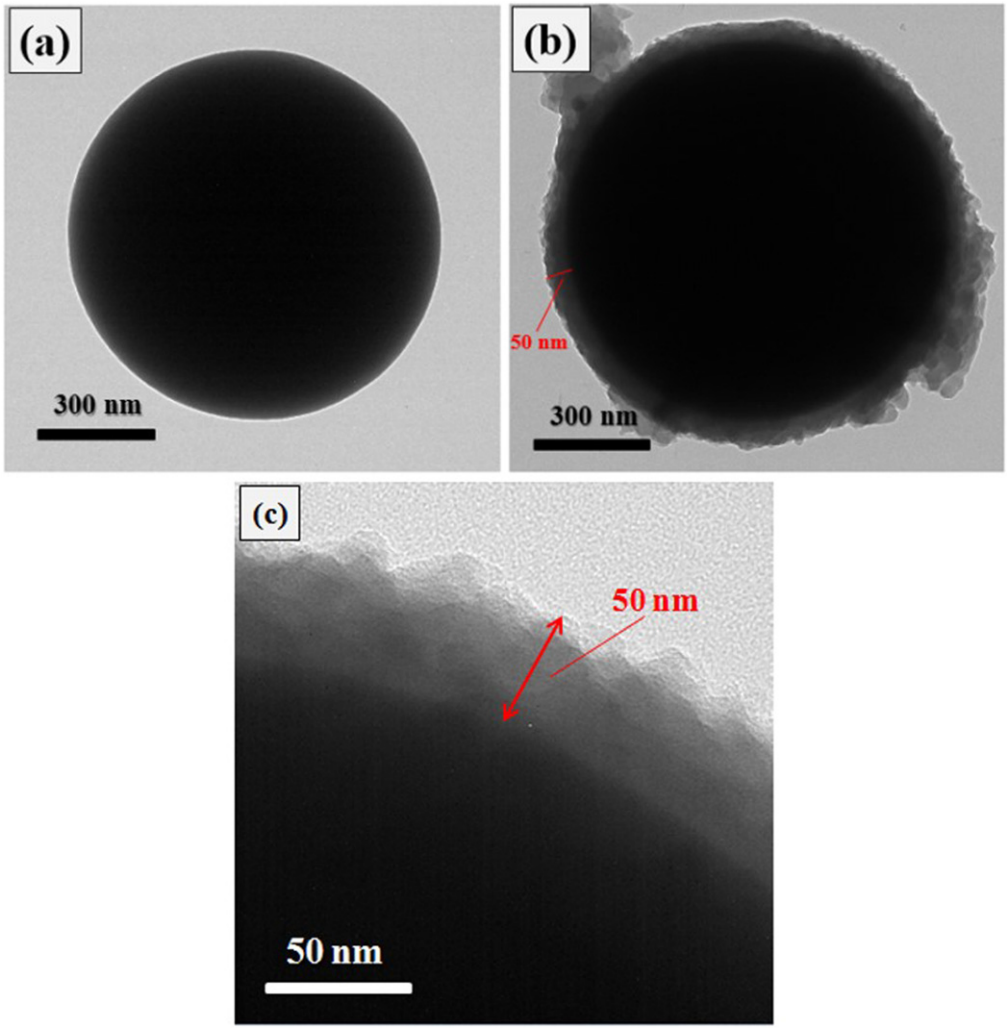

Figure 4. TEM images of the silica/PANI core–shell microspheres.

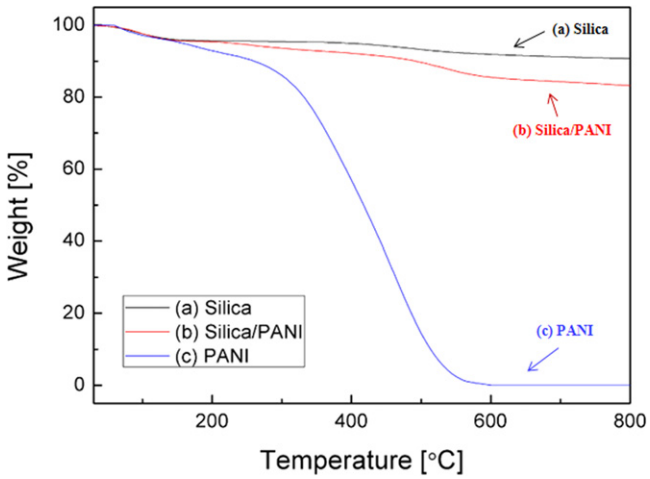

Figure 5. TGA data of pure silica (a), silica/PANI core–shell microspheres (b) and PANI (c).

The electric stimuli-responsive properties of the silica/PANI core–shell microspheres were observed by OM under an applied electric field. The silica/PANI core–shell microsphere-based ER fluid was set between the two sides of the aluminum electrodes and observed by OM, as shown in figure 6. Initially, in the absence of an electric field, the ER particles were dispersed randomly between the two electrodes. Under an electric voltage of 300 V, the particles transformed immediately to a chain-structure parallel to the electric field due to polarization of the particles.

When the particles have high conductivity, electric break-down occurs under high electric field applied. To avoid such an electric break-down problems, silica/PANI core–shell particles were dedoped with a 1 M NaOH solution to reduce the electrical conductivity. Figure 7(a) shows the shear stress versus shear rate for pure silica (closed) and silica/PANI (open) in several electric field strengths, in which a 20 vol% pure silica ER fluid was also prepared for comparison. Newtonian behavior was observed in both fluids in the absence of an electric field. Under the electric field strength, the suspension particles were polarized and formed a chain-structure. Therefore, the ER fluids had a yield stress under the electric field strength. This confirmed that the yield stress of the PANI coating on the surface of silica particles-based ER fluid is higher than that of pure silica-based ER fluid. In

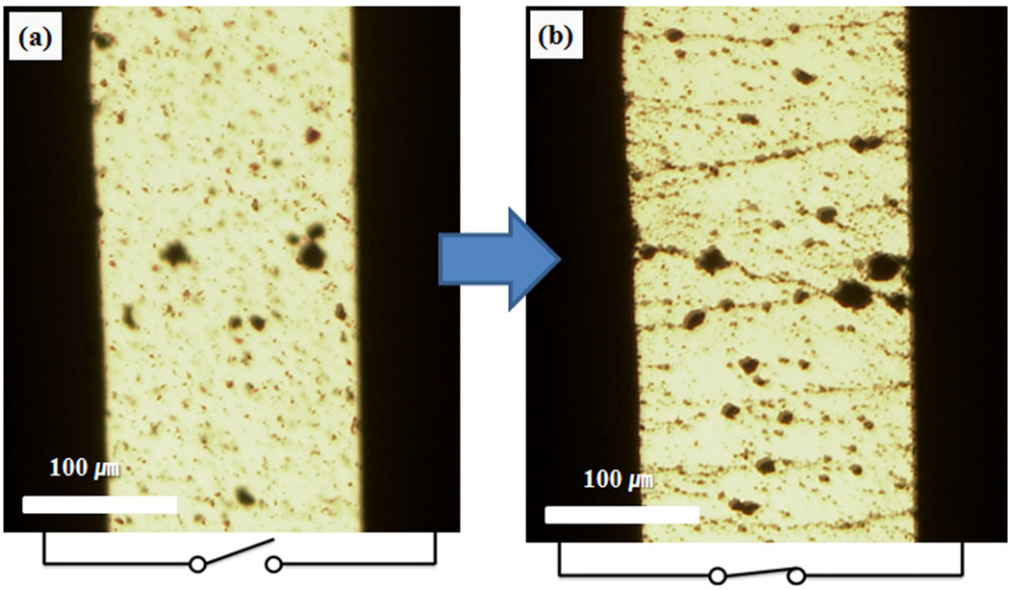

Figure 6. OM image of a silica/PANI core–shell microsphere; (a) 0 V and (b) 300 V.

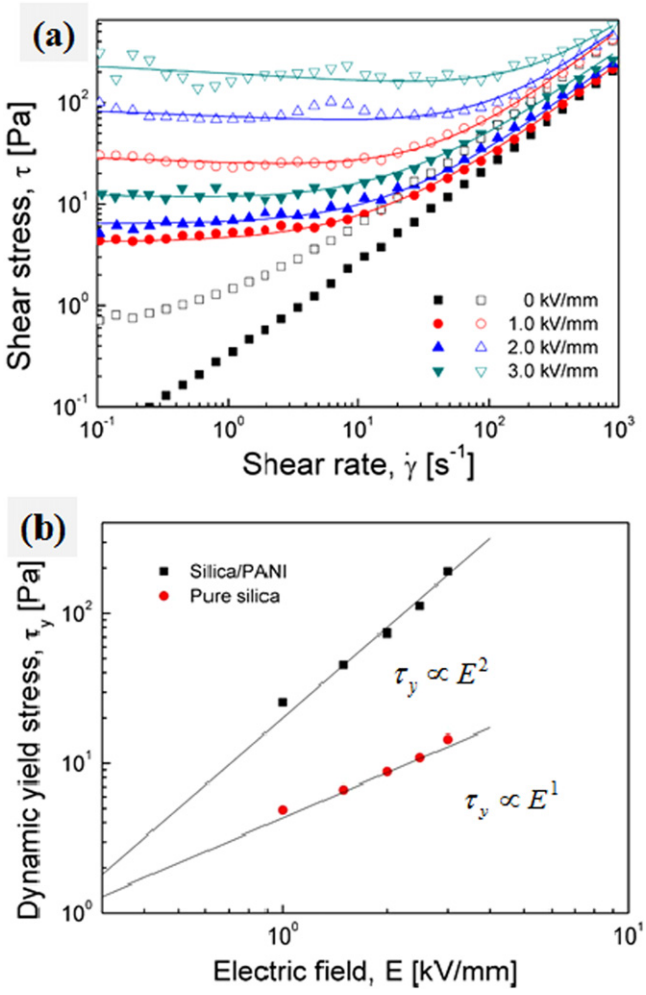

Figure 7. (a) Shear stress as a function of the shear rate for pure silica (closed) and silica/PANI (open) 20 vol% ER fluid under different electric field strengths. (b) Dynamic yield stress of silica/PANI and pure silica-based ER fluids as a function of the electric field strength.

addition, with increasing electric field strength, the yield stress also increased.

On the other hand, to fit the flow curves of figure 7(a), the Cho–Choi–Jhon (CCJ) model [38], which is a more appropriate equation to fit the flow curves of the ER fluids above the entire shear rate region, was adopted, and is described as follows:

$$\tau = \frac{\tau_0}{1 + (t_1\dot{\gamma})^{\alpha}} + \eta_{\infty}\left(1 + \frac{1}{(t_2\dot{\gamma})^{\beta}}\right)\dot{\gamma}, \tag{3}$$

where t_1 and t_2 are time constants, and η_{∞} is the shear viscosity at an infinite shear rate. The parametric exponent, α, implies the tendency of decrease in shear stress at low shear rate regions, whereas β is in the range of 0–1 for the high shear rate region. Table 1 lists the fitting parameters of the ER fluids to the CCJ model.

Figure 7(b) presents the yield stress (τ_0) re-plotted as a function of the electric field strength (E). According to the ER mechanism, the equation for the yield stress and E follows the power law model, $\tau_0 \propto E^m$; the exponent m has a range of values for different ER materials but has an empirical value range of 1.0–2.0 [39, 40]. The exponent values (m) of pure silica and silica/PANI ER fluids were calculated to be 1.0 and 2.0, respectively. Note that the slope of 2.0 follows the polarization model. This suggests that the PANI coating on the surface of silica enhanced the ER effect due to enhanced polarization of particles by forming a chain-structure with a stronger interaction than that of pure silica.

Figure 8(a) shows shear viscosity versus shear rate for pure silica (closed) and silica/PANI (open) at several electric field strengths. Newtonian fluid behavior was observed in the absence of an electric field. When the electric field strength was applied, the zero shear viscosity was increased due to the formation of a chain-structure. In addition, shear thinning behavior, which is a decrease in the shear viscosity with increasing shear rate, appeared above the entire shear rate

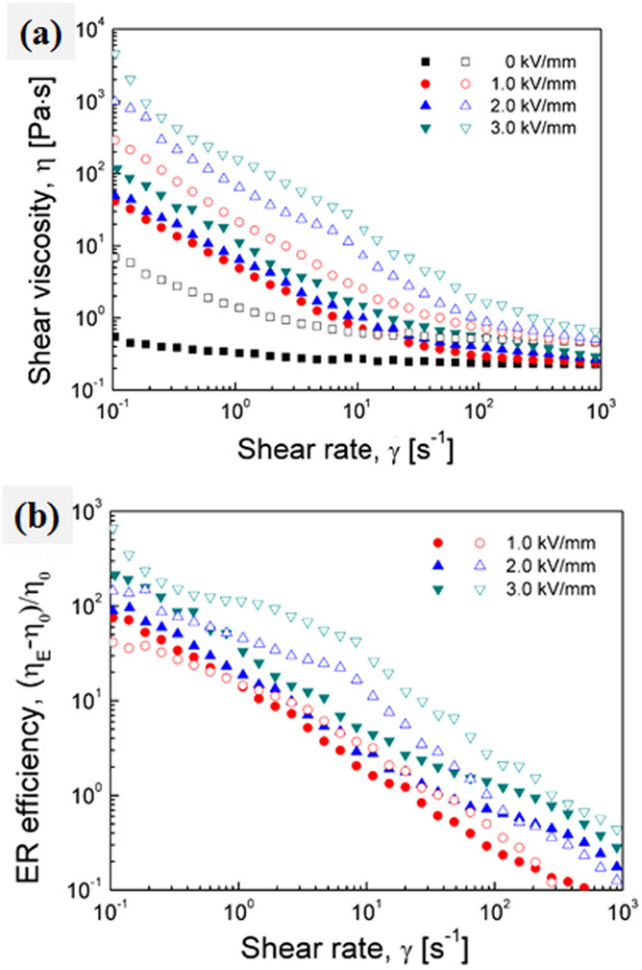

Figure 8. Shear viscosity (a) and ER efficiency (b) as a function of the shear rate for pure silica (closed) and silica/PANI (open) 20 vol% ER fluids under different electric field strength.

region. Under the same electric field strength, the shear viscosity of the silica/PANI-based ER fluid was observed to be higher than that of the pure silica-based ER fluid. The ER efficiency is another significant factor in ER systems, which evaluates the change in the system both in the absence and presence of an external electric field. This can be calculated as follows [41]:

$$e = \frac{(\eta_E - \eta_0)}{\eta_0}, \tag{4}$$

where η_E is a viscosity in the presence of an electric field and η_0 is the field-off viscosity. Figure 8(b) shows the dependence of the ER efficiency on the shear rate. With increasing electric field strength, the ER efficiency also increased, whereas the differences in the two ER fluids were reduced due to the dominance of hydrodynamic forces at high shear rates.

Dynamic-oscillation tests were performed to reveal the viscoelastic properties of the ER fluids. The limit of the linear viscoelastic range was determined in the strain amplitude sweep at an angular frequency of 6.28 rad s^{-1}. Figure 9 shows the storage modulus as a function of strain under different electric field strengths for pure silica and silica/PANI-based ER fluids. A plateau region was observed where the structural deformation is reversible. To measure the frequency sweep, the strain selected was in the linear viscoelastic region. When the strain exceeds the linear viscoelastic region, the storage and loss modulus decrease due to the irreversible change in structure. Therefore, the critical strain in the plateau region was 0.000 05 for the frequency sweep. In addition, a different representation of the strain amplitude sweep data is to plot the strain dependence of the in-phase (elastic) component of the total stress $G'\gamma_0$ (figure 9(b)). The maxima of the elastic stress provide a quantitative way of localizing the shear yield points. The yield stresses were plotted as a function of the applied electric field strength and compared with dynamic yield stress in figure 9(c). The elastic yield stress was slightly higher than that of the dynamic yield stress. This also depends on the power law model, and the value of α is 2, which is the same value as the dynamic yield stress.

Figures 10(a) and (b) show the storage and loss modulus versus the angular frequency for ER fluids at a strain of 0.0005. The storage modulus, which is a measure of the elastic property, was higher than the loss modulus, which is a

Table 1. Optimal parameters in the CCJ model fitting of the flow curves of pure silica and silica/PANI core–shell microsphere-based ER fluids for different electric field strengths.

		Electric field strength		
ER fluid	Parameters	1.0 kV mm^{-1}	2.0 kV mm^{-1}	3.0 kV mm^{-1}
Silica	τ_0	4.2	8.3	12.4
	t_1	0.000 001	0.000 001	0.000 001
	α	0.5	0.1	0.1
	β	0.3	0.3	0.3
	$\eta\infty$	0.238	0.267	0.291
	t_2	0.5	0.5	0.5
Silica/PANI	τ_0	24	71	187
	t_1	0.1	0.02	0.05
	α	0.5	0.6	0.6
	β	0.8	0.8	0.8
	$\eta\infty$	0.45	0.5	0.647
	t_2	0.02	0.02	0.02

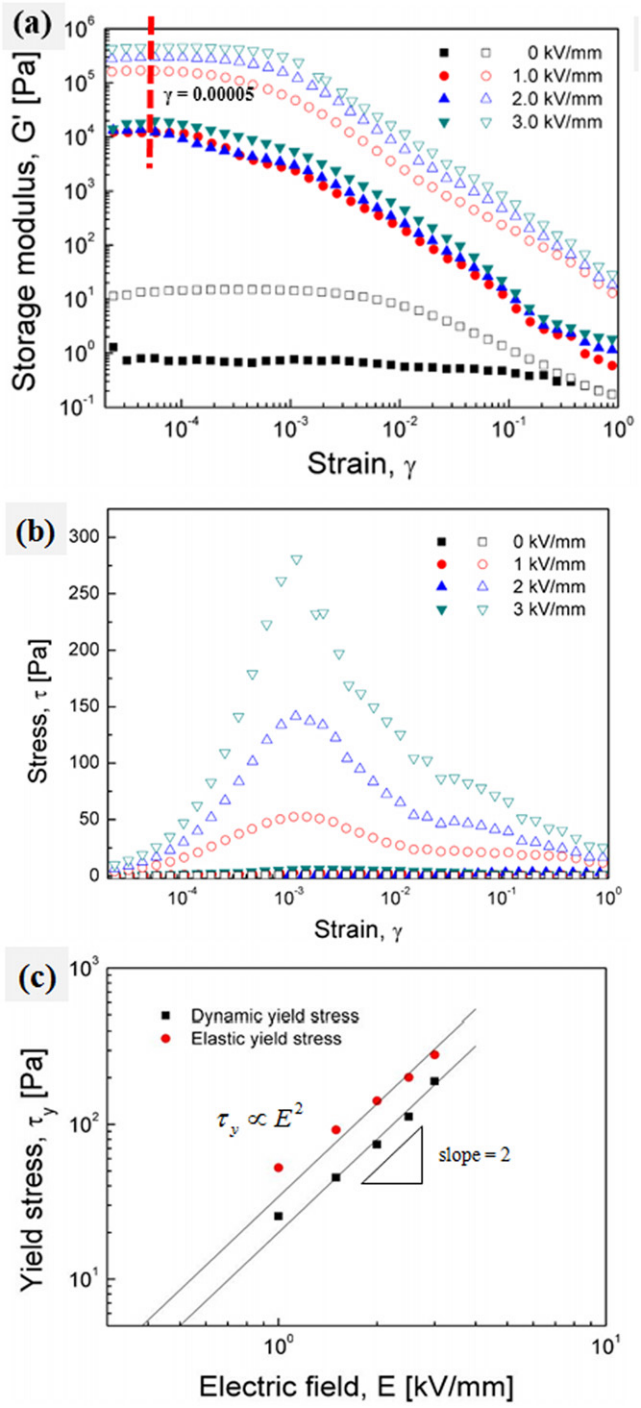

Figure 9. (a) Storage modulus and (b) stress as a function of strain for pure silica and silica/PANI 20 vol% ER fluids under different electric field strengths: pure silica (closed), silica/PANI (open). (c) Fitting line to the dynamic and elastic yield stresses (points).

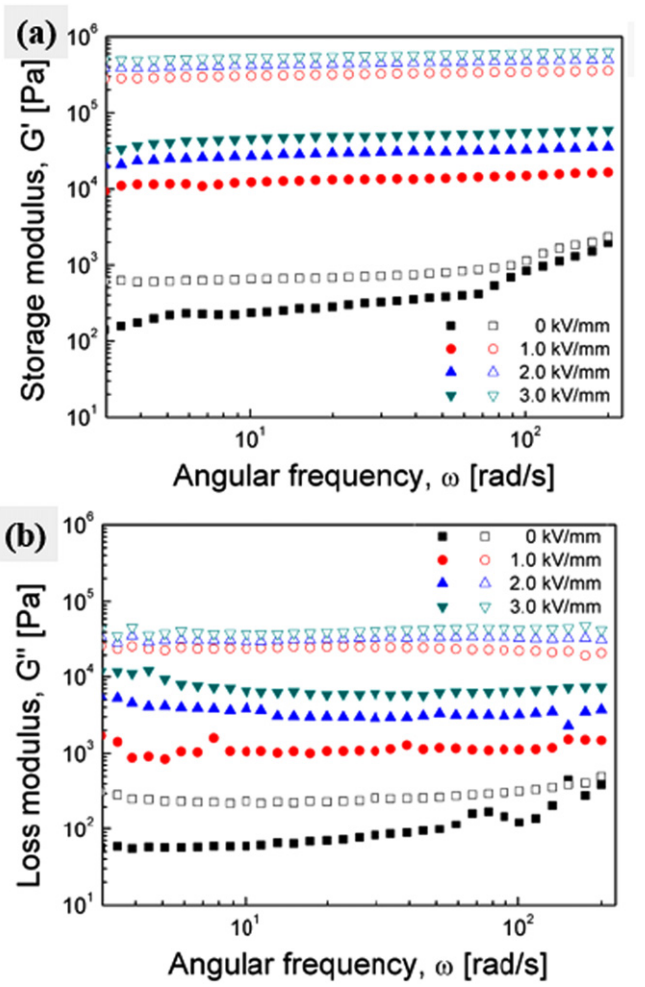

Figure 10. Storage modulus (a) and loss modulus (b) as a function of the angular frequency for pure silica and silica/PANI 20 vol% ER fluids under different electric field strengths: pure silica (closed), silica/PANI (open).

measure of the viscous property [13]. The results indicated the domination of the elastic behaviors over viscous behaviors in the ER fluids. The storage modulus of the silica/PANI-based ER fluid was higher than the storage modulus of the pure silica-based ER fluid above the entire angular frequency region. This suggests a strong interaction among particles due to the PANI coating on the surface of silica.

The solid-like characteristics of the ER fluids could be also confirmed by examining the stress relaxation behavior. The stress relaxation is difficult to measure directly because of the intrinsic characteristics of suspensions and the limitation of the mechanical measurements arising from the equipment itself. Therefore, it was calculated from the dynamic modulus data. The stress relaxation modulus [$G(t)$] was calculated from the values of $G'(\omega)$ and $G''(\omega)$ in figure 9 using the numerical formula, which is known as the Schwarzl equation given as follows [42, 43]:

$$G(t) \cong G'(\omega) - 0.560G''(\omega/2) + 0.200G''(\omega). \quad (5)$$

From this equation, the very short-time relaxation behavior of the material [43] can be predicted, and the result of the calculation is shown in figure 11. In the absence of an electric field, the relaxation modulus decreased slightly and exhibited liquid-like behavior. When the electric field was applied, there is no stress relaxation due to the solid-like behavior.

To observe the sensitivity and stability of the silica/PANI-based ER fluid, the steady shear flow was operated

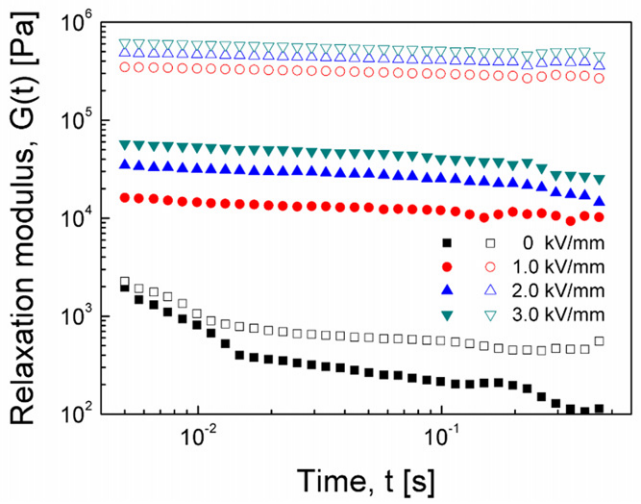

Figure 11. Relaxation modulus $G(t)$ of pure silica and silica/PANI 20 vol% ER fluids as calculated form $G'(\omega)$ and $G''(\omega)$ under differe'nt electric field strengths: pure silica (closed), silica/PANI (open).

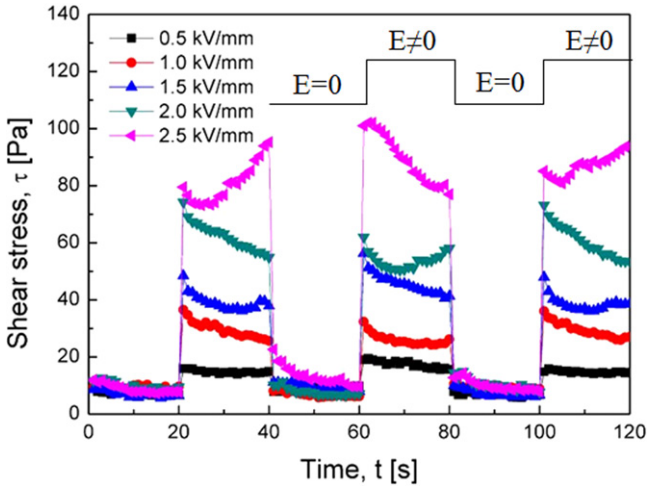

Figure 12. Shear stress of the silica/PANI-based 20 vol% ER fluid at a fixed shear rate of 1 s^{-1} under various electric field strengths, with a square voltage pulse ($t = 20$ s).

with a square voltage pulse ($t = 20$ s). In figure 12, the shear stress was measured at a fixed shear rate of 1.0 (1 s^{-1}) in various electric fields. The shear stress increased immediately under an applied external electric field. Similarly, the shear stress decreased rapidly to the zero-field level when the electric field was removed. These characteristics highlight the sensitive, reversible good control by the electric field, making it suitable for the application of ER materials.

The dielectric properties are another important characteristic of an ER fluid regarding their rate of interfacial polarization. Figures 13(a) and (b) present the dielectric spectra as a function of the frequency (ω) and Cole–Cole plots for silica/PANI-based ER fluid, respectively. The permittivity decreased with increasing frequency and the dielectric loss factor showed a peak at a specific frequency. The dielectric spectra of pure silica particle based ER suspension could be referred from our previous results, demonstrating its inferior dielectric characteristics compared with that of ammonium persulfate coated silica microspheres [44]. The line in figure 13(b) was obtained by fitting the data to the Cole–Cole formula [45, 46], which can be expressed as

$$\varepsilon^* = \varepsilon' - \mathrm{i}\varepsilon'' = \varepsilon_\infty + \frac{\Delta\varepsilon}{1 + (\mathrm{i}\omega\lambda)^{1-\alpha}}, 0 \leqslant \alpha \leqslant 1, \quad (6)$$

where ε_0 is ε' at $\omega \to 0$ and ε_∞ is ε' at $\omega \to \infty$. λ is the relaxation time of interfacial polarization and $\Delta\varepsilon = \varepsilon_0 - \varepsilon_\infty$ indicates the achievable polarizability of the particles in the ER fluid [46–48]. The exponent, $(1 - \alpha)$, means the broadness of the relaxation time distribution [49].

Table 2 lists the fitting parameters for equation (4). These results indicate that the particles respond rapidly to polarization under an applied electric field.

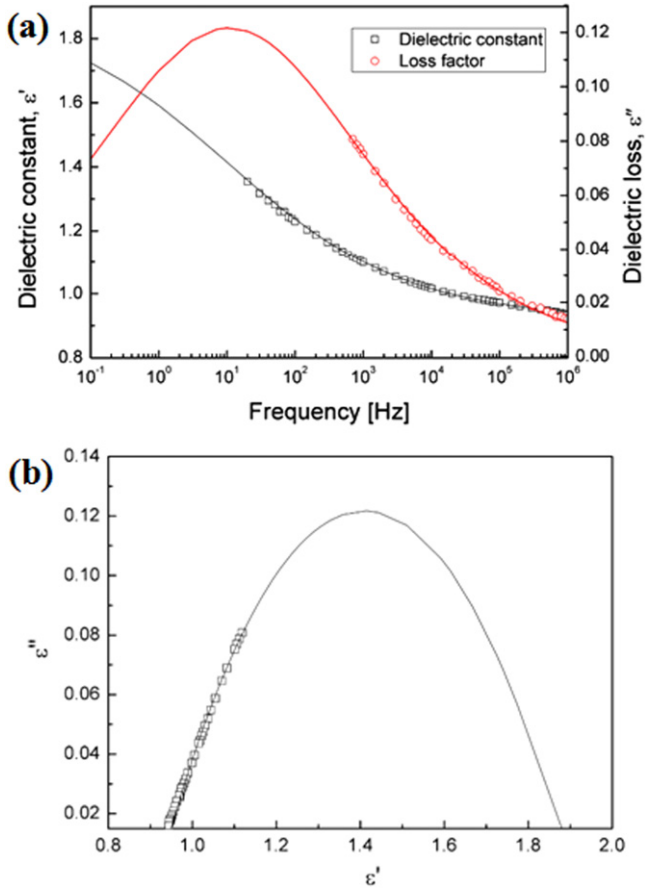

Figure 13. Dielectric spectra (a) and Cole–Cole fitting curve (b) of silica/PANI core–shell microsphere-based ER fluid.

Table 2. Parameters in equation (6).

Parameters	ε_0	ε_∞	$\Delta\varepsilon = \varepsilon_0 - \varepsilon_\infty$	λ	$1-\alpha$
Value	1.90	0.92	0.98	0.015	0.69

4. Conclusion

For the PANI coating on the silica surface, the pure silica was modified by PAPTMS to activate an aniline group on the silica surface. The silica/PANI core–shell microspheres were synthesized by dispersion polymerization and π–π^* stacking interactions between the aniline functional group and aniline monomer. The PANI-coated silica surface was rough, whereas the pure silica surface was very smooth. The shell thickness was approximately 15 nm. The ER properties of silica/PANI microspheres-based ER fluid showed relatively higher viscosity, shear stress, storage modulus and yield stress than those of the pure silica-based ER fluid. Moreover, the shear stress curves could be fitted to the CCJ model.

Acknowledgments

This work was supported by a research grant from National Research Foundation, Korea (NRF-2013R1A1A2057955).

References

[1] Dai R, Wu G and Chen H 2011 Stable titanium dioxide grafted with poly [N-(p-vinyl benzyl) phthalimide] composite particles in suspension for electrophoretic displays *Colloid Polym. Sci.* **289** 401–7

[2] Wang J and Yang X 2007 Raspberry-like polymer/silica core-corona composite by self-assemble heterocoagulation based on a hydrogen-bonding interaction *Colloid Polym. Sci.* **286** 283–91

[3] Yilmaz H, Unal H I and Sari B 2007 Synthesis, characterization and electrorheological properties of poly(o-toluidine)/Zn conducting composites *J. Appl. Polym. Sci.* **103** 1058–65

[4] Chen W, Liu X, Liu Y and Kim H I 2010 Synthesis of microcapsules with polystyrene/ZnO hybrid shell by pickering emulsion polymerization *Colloid Polym. Sci.* **288** 1393–9

[5] Izu N, Uchida T, Matsubara I, Itoh T, Shin W and Nishibori M 2011 Formation mechanism of monodispersed spherical core–shell ceria/polymer hybrid nanoparticles *Mater. Res. Bull.* **46** 1168–76

[6] Manuel J, Raghavan P, Shin C, Heo M Y, Ahn J H, Noh J P, Cho G B, Ryu H S and Ahn H J 2010 Electrosprayed polyaniline as cathode material for lithium secondary batteries *Mater. Res. Bull.* **45** 265–8

[7] Cheng Q, Pavlinek V, He Y, Li C and Saha P 2009 Electrorheological characteristics of polyaniline/titanate composite nanotube suspensions *Colloid Polym. Sci.* **287** 435–41

[8] Plachy T, Sedlacik M, Pavlinek V and Stejskal J 2015 The observation of a conductivity threshold on the electrorheological effect of p-phenylenediamine oxidized with p-benzoquinone *J. Mater. Chem.* C **3** 9973–80

[9] Zhang W L and Choi H J 2012 Silica–graphene oxide hybrid composite particles and their electroresponsive characteristics *Langmuir* **28** 7055–62

[10] Wang Y, Zou B, Gao T, Wu X, Lou S and Zhou S 2012 Synthesis of orange-like Fe_3O_4/PPy composite microspheres and their excellent Cr(vi) ion removal properties *J. Mater. Chem.* **22** 9034–40

[11] Xu Z H, Feng B, Bian S S, Liu T, Wang M L, Gao Y, Sun D, Gao X and Sun Y G 2012 Monodisperse and core–shell structured SiO_2@Lu_2O_3:Ln($^{3+}$) (Ln = Eu, Tb, Dy, Sm, Er, Ho, and Tm) spherical particles: a facile synthesis and luminescent properties *J. Solid State Chem.* **196** 301–8

[12] Hong J Y and Jang J 2010 A comparative study on electrorheological properties of various silica-conducting polymer core–shell nanospheres *Soft Matter* **6** 4669–71

[13] Liu Y D and Choi H J 2012 Electrorheological fluids: smart soft matter and characteristics *Soft Matter* **8** 11961

[14] Kim Y D and Kee D 2007 Measuring static yield stress of electrorheological fluids using the slotted plate device *Rheol. Acta* **47** 105–10

[15] Tsuda K, Hirose Y, Ogura H and Otsubo Y 2010 Motion control of pattern electrode by electrorheological fluids *Colloids Surf.* A **360** 57–62

[16] Liu Y, Davidson R and Taylor P 2005 Touch sensitive electrorheological fluid based tactile display *Smart Mater. Struct.* **14** 1563–8

[17] Cheng Q, Pavlinek V, Lengalova A, Li C, He Y and Saha P 2006 Conducting polypyrrole confined in ordered mesoporous silica SBA-15 channels: preparation and its electrorheology *Micropor. Mesopor. Mater.* **93** 263–9

[18] Zhang W L, Park B J and Choi H J 2010 Colloidal graphene oxide/polyaniline nanocomposite and its electrorheology *Chem. Commun.* **46** 5596–8

[19] Ozkan S, Unal H I, Yilmaz E and Suludere Z 2015 Electrokinetic and antibacterial properties of needle like-TiO_2/polyrhodanine core/shell hybrid nanostructures *J. Appl. Polym. Sci.* **132** 41554

[20] Marins J A, Giulieri F, Soares B G and Bossis G 2013 Hybrid polyaniline-coated sepiolite nanofibers for electrorheological fluid applications *Synth. Met.* **185** 9–16

[21] Kim M J, Liu Y D and Choi H J 2014 Urchin-like polyaniline microspheres fabricated from self-assembly of polyaniline nanowires and their electro-responsive characteristics *Chem. Eng. J.* **235** 186–90

[22] Zhou Y, Qin Z Y, Li L, Zhang Y, Wei Y L, Wang L F and Zhu M F 2010 Polyaniline/multi-walled carbon nanotube composites with core–shell structures as supercapacitor electrode materials *Electrochim. Acta* **55** 3904–8

[23] Yeh J M, Kuo T H, Huang H J, Chang K C, Chang M Y and Yang J C 2007 Preparation and characterization of poly(o-methoxyaniline)/Na^+–MMT clay nanocomposite via emulsion polymerization: electrochemical studies of corrosion protection *Eur. Polym. J.* **43** 1624–34

[24] Dey A, De S, De A and De S K 2004 Characterization and dielectric properties of polyaniline–TiO_2 nanocomposites *Nanotechnology* **15** 1277–83

[25] Lei X and Su Z 2007 Conducting polyaniline-coated nano silica by in situ chemical oxidative grafting polymerization *Polym. Adv. Technol.* **18** 472–6

[26] Lengálová A, Pavlínek V R, Sáha P, Stejskal J, Kitano T and Quadrat O 2003 The effect of dielectric properties on the electrorheology of suspensions of silica particles coated with polyaniline *Physica* A **321** 411–24

[27] Sasidharan M, Mal N K and Bhaumik A 2007 In-situ polymerization of grafted aniline in the channels of mesoporous silica SBA-15 *J. Mater. Chem.* **17** 278–83

[28] Kuramoto N, Yamazaki M, Nagai K, Koyama K, Tanaka K, Yatsuzuka K and Higashiyama Y 1994 Electrorheological property of a polyaniline-coated silica suspension *Thin Solid Films* **239** 169–71

[29] Takei T, Yoshimura K, Yonesaki Y, Kumada N and Kinomura N 2005 Preparation of polyaniline/mesoporous silica hybrid and its electrochemical properties *J. Porous Mater.* **12** 337–43

[30] Dai C F, Weng C J, Chien C M, Chen Y L, Yang S Y and Yeh J M 2013 Using silane coupling agents to prepare

raspberry-shaped polyaniline hollow microspheres with tunable nanoshell thickness *J. Colloid Interface Sci.* **394** 36–43

[31] Yin J, Xia X, Xiang L and Zhao X 2010 Coaxial cable-like polyaniline@titania nanofibers: facile synthesis and low power electrorheological fluid application *J. Mater. Chem.* **20** 7096–9

[32] Yin J, Xia X, Wang X and Zhao X 2011 The electrorheological effect and dielectric properties of suspensions containing polyaniline@titania nanocable-like particles *Soft Matter* **7** 10978–86

[33] Yin J, Wang X, Chang R and Zhao X 2012 Polyaniline decorated graphene sheet suspension with enhanced electrorheology *Soft Matter* **8** 294–7

[34] Zheng J Z, Zhou X P, Xie X L and Mai Y W 2010 Silica hybrid particles with nanometre polymer shells and their influence on the toughening of polypropylene *Nanoscale* **2** 2269–74

[35] Liu Y D, Park B J, Kim Y H and Choi H J 2011 Smart monodisperse polystyrene/polyaniline core–shell structured hybrid microspheres fabricated by a controlled releasing technique and their electro-responsive characteristics *J. Mater. Chem.* **21** 17396–402

[36] Zhang W L, Piao S H and Choi H J 2013 Facile and fast synthesis of polyaniline-coated poly(glycidyl methacrylate) core–shell microspheres and their electro-responsive characteristics *J. Colloid Interface Sci.* **402** 100–6

[37] Liu Y D, Kim J E and Choi H J 2011 core–shell structured monodisperse poly(3, 4-ethylenedioxythiophene)/poly (styrenesulfonic acid) coated polystyrene microspheres and their electrorheological response *Macromol. Rapid Commun.* **32** 881–6

[38] Choi H J and Jhon M S 2009 Electrorheology of polymers and nanocomposites *Soft Matter* **5** 1562–7

[39] Yin J B and Zhao X P 2008 Electrorheological properties of titanate nanotube suspensions *Colloids Surf.* A **329** 153–60

[40] Cheng Y C, Wu K H, Liu F H, Guo J J, Liu X H, Xu G J and Cui P 2010 Facile approach to large-scale synthesis of 1D calcium and titanium precipitate (CTP) with high electrorheological activity *ACS Appl. Mater. Interf.* **2** 621–5

[41] Yin J B and Zhao X P 2004 Preparation and enhanced electrorheological activity of TiO_2 doped with chromium ion *Chem. Mater.* **16** 321–8

[42] Prasad R, Pasanovic-Zujo V, Gupta R K, Cser F and Bhattacharya S N 2004 Morphology of EVA based nanocomposites under shear and extensional flow *Polym. Eng. Sci.* **44** 1220–30

[43] Schwarzl F R 1975 Numerical calculation of stress relaxation modulus from dynamic data for linear viscoelastic materials *Rheol. Acta* **14** 581–90

[44] Liu Y D, Quan X M, Lee B M, Kim I G and Choi H J 2014 Fabrication of ammonium persulfate coated silica microsphere via chemical grafting and its electrorheology *J. Mater. Sci.* **49** 2618–23

[45] Cole K S and Cole R H 1941 Dispersion and absorption in dielectrics: alternating current characteristics *J. Chem. Phys.* **9** 341–51

[46] Liu Y D, Fang F F and Choi H J 2010 Core–shell structured semiconducting PMMA/polyaniline snowman-like anisotropic microparticles and their electrorheology *Langmuir* **26** 12849–54

[47] Hwang J K, Shin K, Lim H S, Cho J C, Kim J W and Suh K D 2012 The effects of particle conductivity on the electrorheological properties of functionalized MCNT-coated doublet-shaped anisotropic microspheres *Macromol. Res.* **20** 391–6

[48] Mrlik M, Sedlacik M, Pavlinek V, Bober P, Trchová M, Stejskal J and Saha P 2013 Electrorheology of aniline oligomers *Colloid Polym. Sci.* **291** 2079–86

[49] Cho M S, Cho Y H, Choi H J and Jhon M S 2003 Synthesis and electrorheological characteristics of polyaniline-coated poly(methyl methacrylate) microsphere: size effect *Langmuir* **19** 5875–81